

3D or not 3D, that is the question: raypath interferometry in 3D processing

David C. Henley

ABSTRACT

The successful use of the technique we call ‘raypath interferometry’ has been documented in recent years on several 2D datasets. It has been applied not only in situations where near-surface corrections are large and non-stationary, but also where conventional statics solutions based on surface-consistency also work well. The raypath interferometry method is more complex than surface-consistent statics techniques, but because of the more general concept of ‘raypath consistency’, it is able to provide superior surface corrections for seismic data acquired in areas with complex surface conditions, or in situations like converted-wave (PS) imaging where near-surface variations can lead to large, non-stationary surface corrections.

To apply raypath interferometry to 2D data, the usual source (or receiver) gathers are transformed into a domain where raypath can be parametrized as a coordinate of the ensemble, using one of several possible transforms. This process is straightforward for 2D datasets; but extending the notion to 3D requires further consideration. We discuss here some possibilities and demonstrate one approach which seems promising. Introducing the surface azimuth between source and receiver locations, we demonstrate one pathway for extending raypath interferometry to 3D: extending the ‘surface function’ introduced in 2D raypath interferometry from a 2D function of surface location and raypath parameter to a 3D function of surface location, raypath parameter, and azimuth. We show one way of transforming 3D data into a useful raypath domain using the radial trace transform. We then demonstrate the creation of a 3D ‘reference wavefield’ and show that raypath interferometry, even for 3D data, can be implemented as a single cross-correlation and inverse-filter application, just as in the 2D case. Recovering the original 3D traces by reversing the data sorting/transform operation is straightforward. We show that various trace ensembles extracted from the corrected 3D data have no apparent residual statics compared to the same ensembles extracted from the raw data, hence confirming this approach.

INTRODUCTION

Correcting seismic reflection data for the effects of the surface layer of the earth is one of the more fundamental and important steps in processing those data to form usable images of the earth’s subsurface structure. Most procedures assume some model of the surface layer and use the properties of the model to simplify the problem of computing and applying corrections to the seismic data set. Probably the most widely used constraint arising from the near-surface model is that of surface-consistency, in which the near-surface materials are assumed to have a much lower velocity than the deeper layers. Snell’s Law then constrains raypaths through the surface layer to be nearly vertical, so that all raypaths beginning or ending at a surface point are nearly the same, or surface-consistent, and can be assumed to have the same delay time for reflections transmitted through the layer. Another common assumption arising from the near-surface model is

that the material is relatively smoothly varying and free of large-contrast anomalies. For such a model, scattering and other multi-path phenomena can be ignored, and each reflection event transiting the layer is assumed to consist of a single arrival, uncontaminated by short-delay scattered or multi-path arrivals. This means that a seismic trace can be corrected for the near-surface layer simply by time-shifting it by the amount of the delay associated with the near-surface raypath segments at the source and receiver locations for the seismic trace.

The near-surface layer in many parts of the world is simple enough that the single-arrival and surface-consistent assumptions work well and allow various surface correction techniques to be successfully applied. When the velocity of the layer approaches or exceeds that of the underlying layers, the vertical raypath assumption which enables surface-consistency fails, and simultaneously, stationarity fails. In this case, it is no longer possible to correct a seismic trace with a single time shift, since reflections from deeper layers traverse different near-surface raypath segments, with different transit times, than those from shallower layers. Stationarity can also fail when the base of the near-surface layer is steeply inclined, especially for converted waves (Cova et al, 2013a, 2013b, 2014a, 2014b). If the near-surface layer is also complex enough to support scattering or other multi-path arrivals, the single-arrival assumption which enables correction by time-shifting must be replaced by the assumption of an ‘arrival distribution’, which then requires correction by deconvolution (Henley, 2012a).

Raypath interferometry was developed specifically to find and apply surface corrections to seismic traces when either or both of the surface-consistent and single-arrival assumptions are violated (Henley, 2012a). Two basic principles are involved in the technique; finding and applying corrections along ‘common-raypath’ directions, and using a simple form of interferometry to estimate and apply the actual corrections. The common-raypath constraint requires that the input field data be transformed from the usual X-T domain to a ‘raypath’ domain. Although there are several transforms that can achieve this, the Radial Trace Transform was chosen initially because of its exact invertibility and flexible interpolation options (Henley, 2012a). The closely related Snell Ray Transform has also been shown to function well in transforming data to a raypath domain, but it requires some velocity information to function properly (Henley, 2014). Cova (2014b) has shown that the Tau-P transform can also provide an acceptable pathway to a raypath domain, but that its inexact invertibility must be considered.

The optical interferometry principle adapted to derive and apply corrections in the chosen raypath-parameter domain is illustrated in Figure 1. Here, undisturbed wavefronts from a distant source are shown transiting both a slab of uniform material and a slab of the same material with significant shape/density distortions. Comparing the wavefront emerging from the ‘reference’ material slab with that emerging from the ‘distorted’ slab, using cross-correlation, leads to inverse filter functions which can be used to remove the distortions from the distorted wavefront.

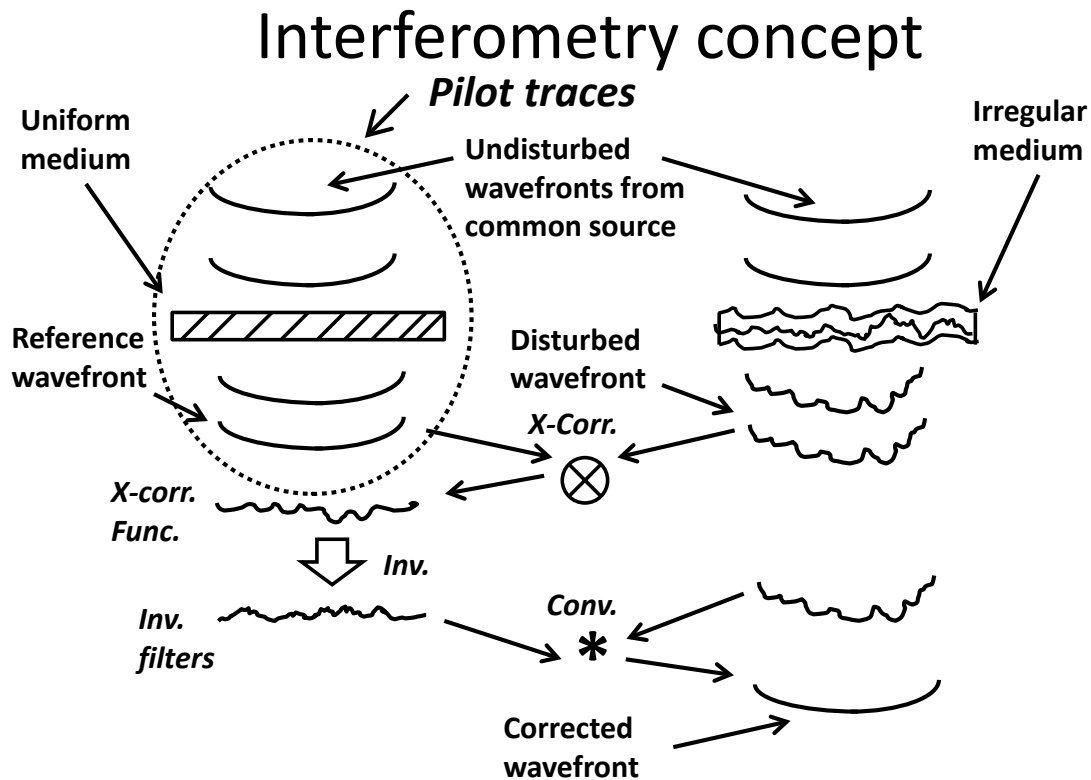


FIG. 1. Schematic portraying a type of optical interferometry. This is the principle implemented in raypath interferometry, where raypath-domain raw seismic traces are cross-correlated against reference wavefield traces to obtain the information needed to correct the raw traces.

In order to adapt this principle to a seismic data volume, we need to create a method for finding a ‘reference wavefront’ from the raw seismic data. As has been shown in earlier work (Henley, 2012a, 2012b, 2014), smoothing gathers of raw seismic traces along specific event horizons, either with simple averaging or SVD methods, leads to usable reference wavefield estimates. Hence, the method known as raypath interferometry consists of the following steps:

- Transform raw shot or receiver trace gathers to a raypath parameter/transit time domain
- Sort the raypath parameter traces to gathers of common raypath parameter
- For each common-raypath-parameter gather, create a reference wavefield estimate
- For each common-raypath-parameter gather, cross-correlate raw traces with corresponding reference wavefield traces
- ‘Condition’ the cross-correlation functions to become surface function estimates

- Derive an inverse filter for each cross-correlation function
- For each common-raypath-parameter gather, apply the corresponding inverse filters to each trace in the gather
- Sort the corrected common-raypath-parameter gathers back to shot or receiver raypath-parameter gathers
- Inverse transform the corrected common-raypath-parameter gathers to corrected shot or receiver gathers

The transform into a raypath-parameter domain is the key step which enables nonstationary surface corrections, since the inverse filters which apply the surface corrections are derived and applied independently for each raypath parameter. Figure 2 illustrates the concept of a ‘surface function’, a short wavelet or time series whose shape embodies all arrivals related to a given reflection, which can vary not only with surface location, but with raypath angle. It is this 2D surface function that we attempt to remove using raypath interferometry. Also in Figure 2, we see how simplifying the near-surface layer to a homogeneous layer with much lower velocity than the underlying layers leads to a 2D surface function that can be well-approximated by a single simple time shift, dependent only upon surface location (the surface-consistency constraint). In recent years we have demonstrated (Henley, 2007a, 2008, 2009, 2011, 2012a, 2012b, 2014), (Cova et al, 2013a, 2013b, 2014a, 2014b) the effectiveness of raypath interferometry, not only on data sets where surface-consistency fails, but on data sets for which conventional statics correction techniques work well, as well as on converted wave (PS) data sets which have large shear-wave statics and which demonstrate obvious nonstationarity.

To date, all of these data sets have been 2D seismic surveys with collinear source and receiver lines, and no attention has been devoted to effects which may not lie in the plane of a conventional 2D seismic section, although Cova et al (2015) explore some procedures necessary to correctly process 2D converted wave data in which sources and receivers are not always collinear. Developing a useful transform procedure to take 3D trace ensembles into a 3D raypath parameter domain is a key step for extending raypath interferometry to 3D seismic data.

Angle-dependent surface function

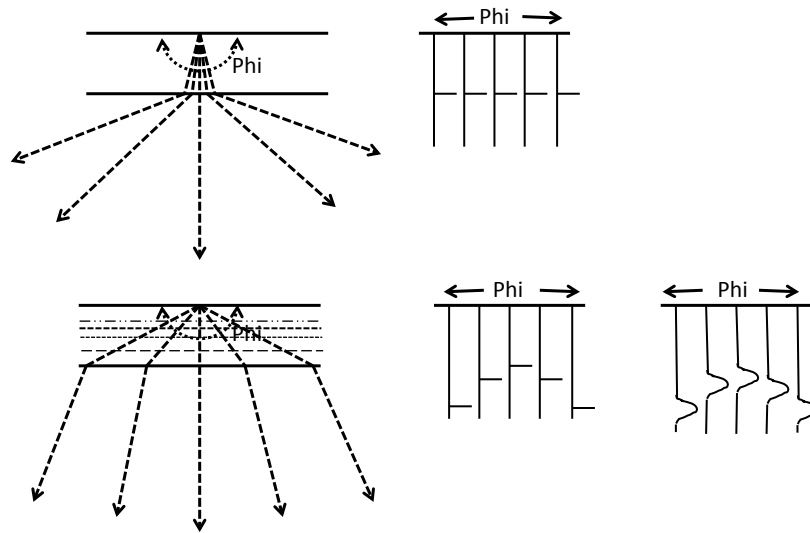


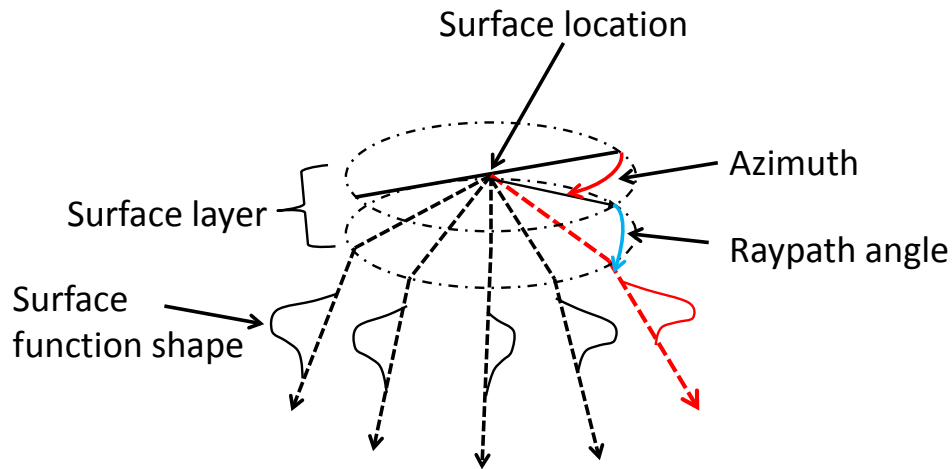
FIG. 2. Schematic illustrating the concept of a 'surface function' dependent upon surface location and raypath angle. Low-velocity, isotropic surface layer leads to surface function with little angular variation (upper diagram), while higher velocity, anisotropic surface layer leads to angular variation and arrival distribution waveforms (lower diagram).

3D CONSIDERATIONS AND COMPLICATIONS

A large proportion of modern seismic reflection data is acquired for the purpose of forming 3D volume images of the subsurface; corrections for near-surface effects are just as important for these much larger data sets as for the simpler 2D surveys. Furthermore, we expect to encounter the same near-surface conditions, in 3D surveys, which lead to failure of surface-consistency and the single reflection arrival constraint. Thus, we need to expand raypath interferometry to the 3D domain in a rational and defensible manner, noting that the geometrical considerations are more complicated than for conventional statics solutions, where surface-consistency can greatly simplify the geometrical and mathematical considerations.

3D surface functions

Whereas static corrections, whether applied to 2D data or 3D data, are one dimensional, the surface functions that we attempt to estimate and remove in raypath interferometry are 2D functions for 2D data, and are coplanar with the 2D image plane. For 3D data, however, the surface functions become 3D, as illustrated in Figure 3, and require an additional dimension (besides surface location and raypath parameter) to characterize them. The most natural additional dimension seems to be source-receiver azimuth, relative to the surface coordinate system for a particular 3D survey. The question is: can we transform and arrange portions of a typical 3D data set with enough redundancy to yield usable 3D surface functions, suitable for application in raypath interferometry?



Surface function shape is the distribution of reflection arrivals and varies with surface location, azimuth, and raypath angle

FIG. 3. Schematic showing the expansion of the 2D surface function into a 3D surface function, dependent upon surface location, raypath angle, and surface azimuth from source to receiver.

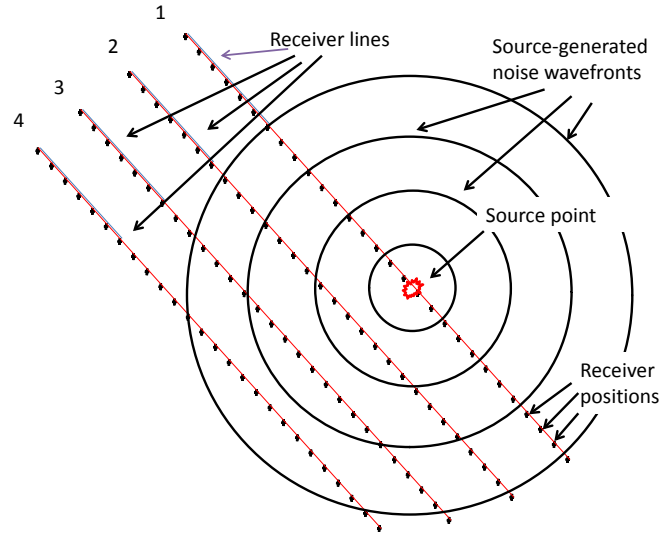
The raypath-parameter domain and data sparsity

Most of the complication involved in extending 2D surface function estimation to 3D surface function estimation occurs in arranging the 3D data set for transforming into the raypath-parameter domain. What we show in this report is an initial attempt to do this in a rational and defensible manner. Furthermore, we explore the use of only the Radial Trace Transform to enter the raypath-parameter domain; the Tau-P Transform is left to other researchers at this point. We do not attempt to create full 3D image volumes, preferring, instead, to compare particular kinds of 2D trace panels as diagnostics.

One of the biggest problems in transforming 3D data is the non-uniformity of the data sampling relative to various coordinates. Henley (2007b) has shown that for the purpose of sampling and attenuating surface waves on 3D source gathers, only the receiver line gather is sampled densely enough to avoid major aliasing of surface waves (Figure 4). Hence, a single receiver line gather can be transformed to the radial trace (RT) domain, with a single raypath parameter associated with each radial trace. The set of RT transforms created from the set of receiver line gathers for a single source then constitutes a kind of raypath-parameter transform for the source—except that the raypaths nearly all lie along different azimuths from source to receiver. As shown by Henley (2007b), if we try to segregate the traces in the original source gather (Figure 5) into azimuthal segments prior to the RT transform (in order to incorporate azimuth as another independent variable), the trace offset distribution is generally too sparse and irregular to yield transforms adequate for the stringent requirements of surface wave estimation.

However, the relatively flat subsurface reflections (body waves) for which we need to find and remove surface effects are much less susceptible to aliasing than surface waves,

and subsequently require a less stringent transform, which may allow us to incorporate azimuth, regardless of the bin population irregularity. Hence we propose to create azimuthal bins which will contain enough traces to allow acceptable RT transforms (no aliasing of reflections) to be computed from source/azimuth/offset trace gathers. These transforms will then be source/azimuth/raypath-parameter gathers.



Coherent noise wavefronts and their relationship to typical 3D seismic acquisition geometry: receiver line spacing \gg receiver spacing

FIG. 4. Schematic showing part of a typical 3D acquisition layout. Receivers are spaced much more closely along receiver lines than in any other direction, making the receiver line gather the obvious domain in which to attack surface waves. Source-receiver azimuths within the receiver line gathers vary widely, however,

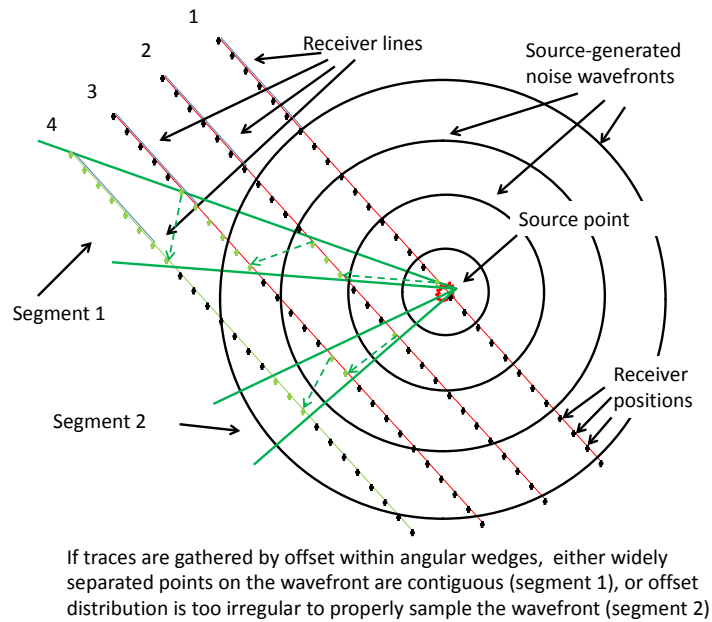


FIG. 5. If we attempt to form gathers based on narrow azimuthal segments, the resulting ensemble populations can be small, and the offset distributions quite irregular, leading to widely variable results in the raypath domain. This does not fulfil requirements for surface wave estimation.

Once we have transformed a 3D data set into a suitable 3D raypath-parameter domain, it should be relatively straightforward to sort the data along one coordinate or another, and to do reference wavefield estimation, cross-correlation, and inverse filtering, as described above. Creating the reference wavefield is a key step, and we will test at least two approaches. With an appropriate wavefield estimate, we should be able to apply a 3D surface correction with only a single inverse filter per raypath.

The Blackfoot data set and test conditions

To test our ideas, we needed a full 3D data set with reasonably good surface coverage, good data quality, and visible statics on reflection events. The well-known 1995 Blackfoot 3C-3D survey (Lawton, 1996, Simin et al, 1996) seemed appropriate and allows the option of processing not only vertical component (PP) data, but also the inline horizontal component (PS). It is large enough to be realistic, but not so large that processing times would be prohibitive, consisting of about 10^6 traces for each component. Another convenient feature of this data set is that there is very little structure over the area of the survey—reflection events are nearly flat, which means that most apparent deviations from flatness can be approximately attributed to the surface effects.

Because our experimental processing, particularly the RT transform, destroys or disrupts trace header information, processing the 3D data set to a complete image volume for testing purposes was not attempted at this time—for diagnostic purposes, comparing smaller, more manageable subsets of the data was more realistic, until we determine a relatively robust processing flow for raypath interferometry in 3D.

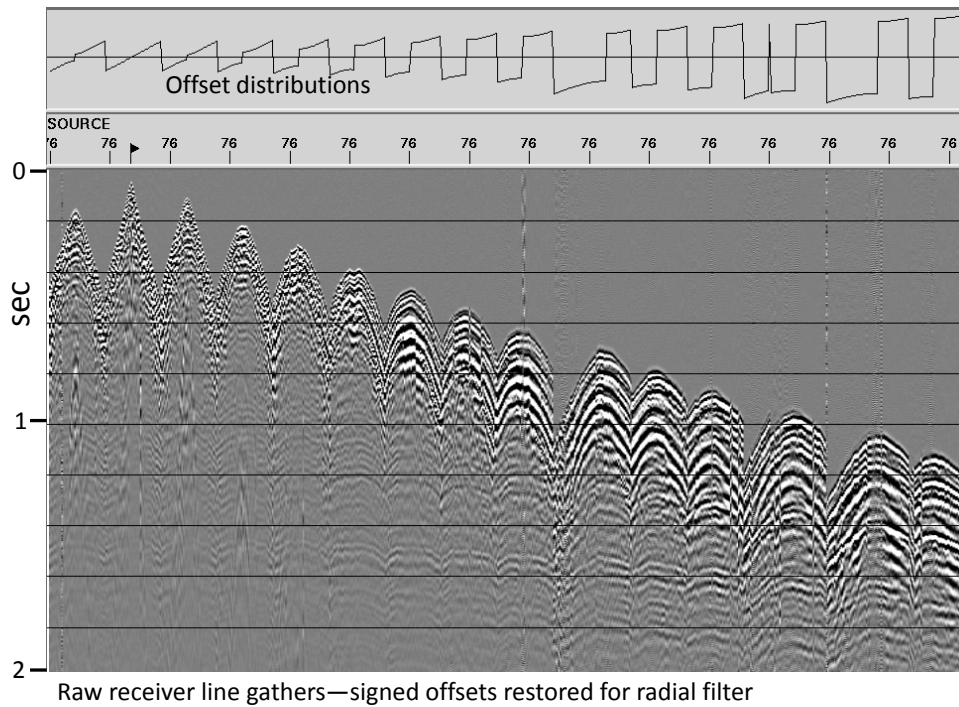


FIG. 6. One source gather from the Blackfoot 3D 3C survey, showing the individual receiver line gathers. Note the strong ground roll noise (hyperbolic on receiver line gathers because of the non-uniform offset distributions for the receiver lines). The trace header plot shows the signed offset plotted for each receiver line gather, as restored by the 'rad3d' process. The large offset 'jump' at the apex of each gather reflects the offset polarity change at the nearest shot position.

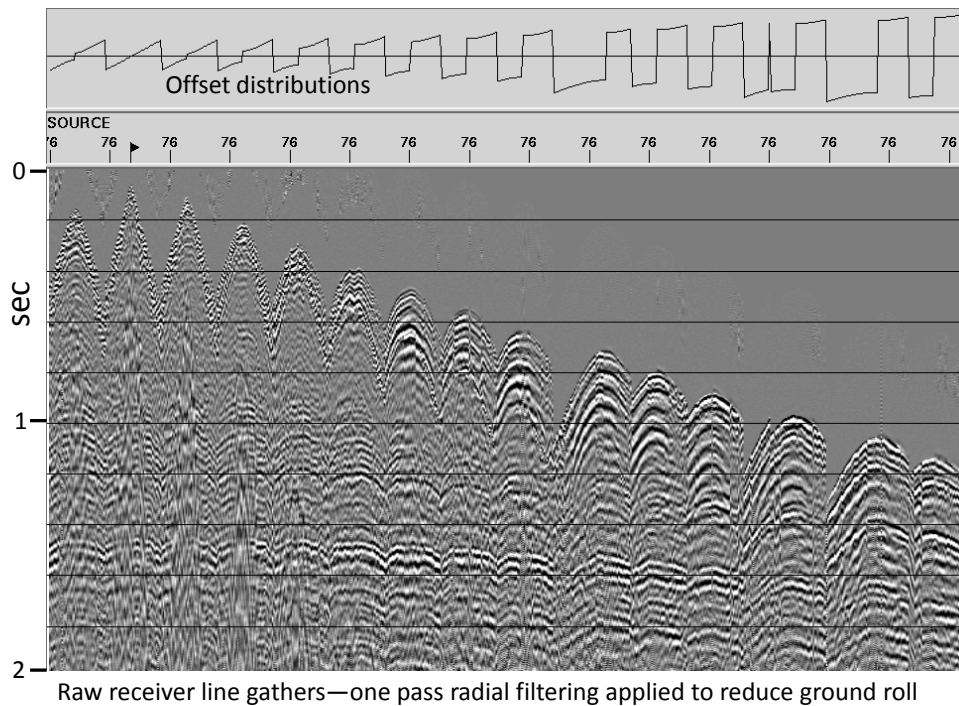


FIG. 7. The Blackfoot source gather from Figure 6 after one pass of RT fan filtering to reduce the ground roll. Reflections at all levels are now more visible than in Figure 6.

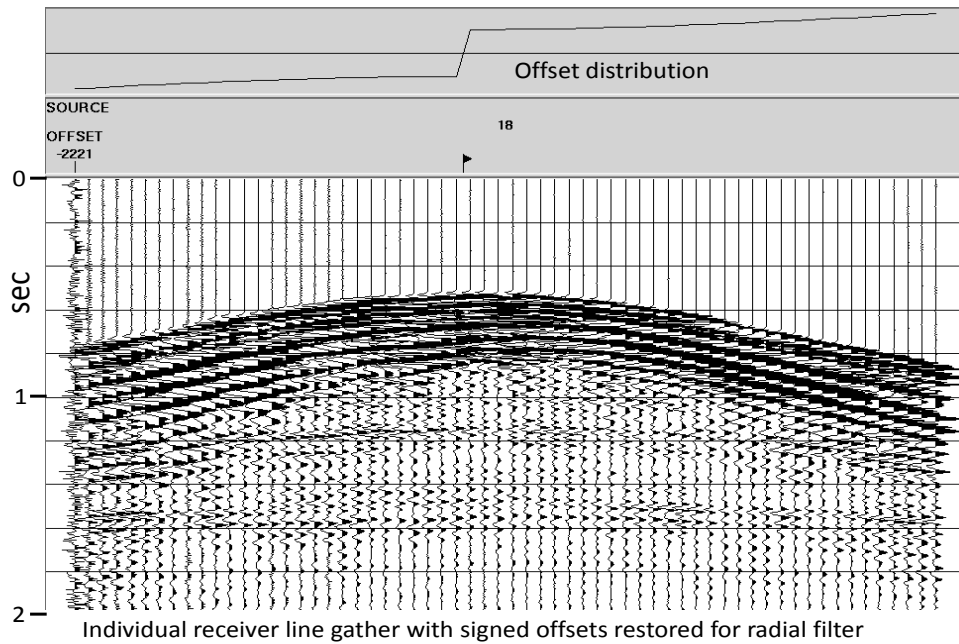


FIG. 8. One receiver line gather from source gather 76 before application of RT filtering.

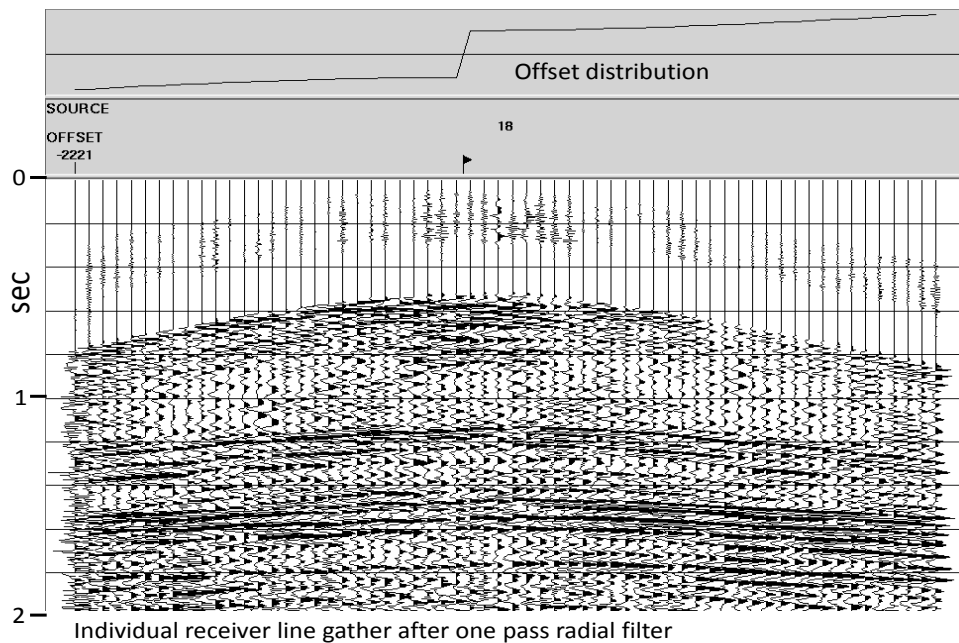


FIG. 9. Receiver line gather from Figure 8 after one pass of RT fan filter.

PROCESSING DETAILS

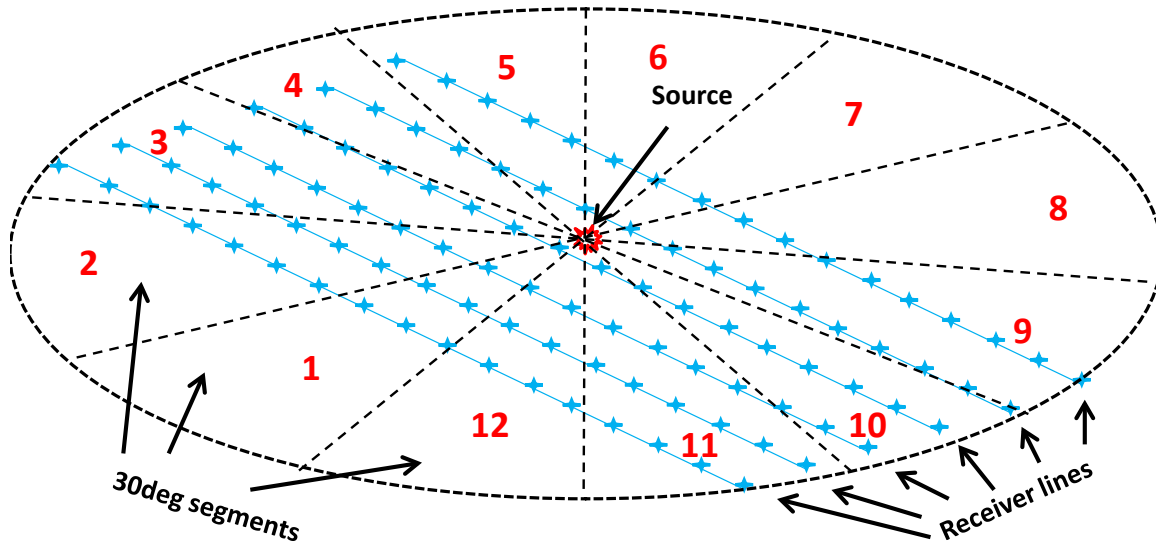
Pre-processing—noise attenuation

Figure 6 shows a full shot gather for source number 76 of the Blackfoot 3D 3C survey. The data displayed are vertical component (PP) data arranged by receiver line. The header plot shows the source-receiver offsets after being modified by the rad3d process for input to the radial trace filter module. This procedure restores the ‘signed offset’

values to the trace headers by projecting the source position perpendicular to each receiver line, then negating all offsets to the low-numbered side of each receiver-line gather. As well, the receiver-line gathers are established as ensembles by setting the appropriate ‘end-ensemble’ flags. This allows the radial trace filter module to process each receiver-line gather as if it were a split-spread 2D source gather (Henley, 2007b), which is the most appropriate way in which to attenuate surface-wave noise. After fixing the headers on the entire 3D data set, we applied a simple radial trace fan filter to all the receiver line gathers to attenuate ground roll, which appears as strong hyperbolic events at the beginning of the long-offset receiver-line gathers and steeply dipping low-frequency events in the centres of the shorter-offset receiver-line gathers. In Figure 6, this noise dominates the records, although deeper reflections can be seen on all gathers. Figure 7 shows the same gathers after one pass of a radial trace fan filter. While ground roll near the apices of the longer-offset receiver-line gathers is not greatly attenuated, energy in the limbs of the noise hyperbolae is considerably reduced, and all legitimate reflections are much more visible. Figures 8 and 9 show a single receiver-line gather before and after radial trace filtering. At this stage, the data are prepared for further processing by creating several new trace headers to assist with sorting and arranging the data into ensembles selected by any of several possible combinations of trace headers.

Pre-processing—trace headers

The header modifications we apply via *rad3d* include a new set of source and receiver coordinates for each trace, where the new coordinates are ‘rotated’ from the survey coordinates to be aligned with the perpendicular from each source to its receiver lines. In addition, a new set of end-ensemble trace headers is created to flag the ends of receiver-line ensembles. Some of the additional headers created to be used in sorting and gathering ensembles include integer source coordinates and the differences between source and receiver coordinates. Two key trace headers created are the source-receiver azimuth, relative to the survey coordinates (rotated to be orthogonal to the perpendicular distance from source to receiver lines), and the azimuth bin number (integer) created from the azimuth (real).



Bins consist of segments 1 + 7, 2 + 8, 3 + 9, 4 + 10, 5 + 11, and 6 + 12

FIG. 10. Diagram showing the proposed binning scheme for creating azimuthally oriented gathers with reasonable populations and offset distributions. As shown in Figures 11-14, azimuthal segments need to be about 30deg in width in order to include enough traces to create reasonable trace populations for RT transformation to the raypath-parameter domain.

Figure 10 is a schematic showing the proposed method for binning raw input 3D source gathers prior to the RT transform. Note that we create 12 azimuth segments, or bins, spanning 360deg, so that each segment includes 30deg. Although this seems like quite a coarse bin size, we found that for the Blackfoot data set, any attempt at finer binning led to unacceptably sparse gathers, even for body waves. Figures 11-14 show a single source gather binned by azimuth, where the bin width ranges from 3deg to 30deg. In each case, NMO has been applied to flatten apparent reflections. What is evident from these figures is that while not much more than half the range of azimuth bins is well-populated for the 3deg bin width, this proportion increases to over 90% for the 30deg bin width. In all cases, the least-populated bins represent azimuth directions rotated 180deg from the most-populated ones. For a shot gather like that of shot 76 in the figures, the source point is not centered in the patch of receiver lines (similar to schematic Figure 5), so it is obvious why certain azimuths are under-represented. For this reason, we decided ad hoc to combine bins aligned at 180deg with respect to each other (the azimuths are thus roughly collinear). When we do this for the source gather at source point 76, the bin populations are as shown in Figure 15, in which we consider the bins now well enough populated to perform reasonable RT transforms. Note that the reflections show many visible deviations from flatness—the surface function effects, or ‘statics’ that we will attempt to correct.

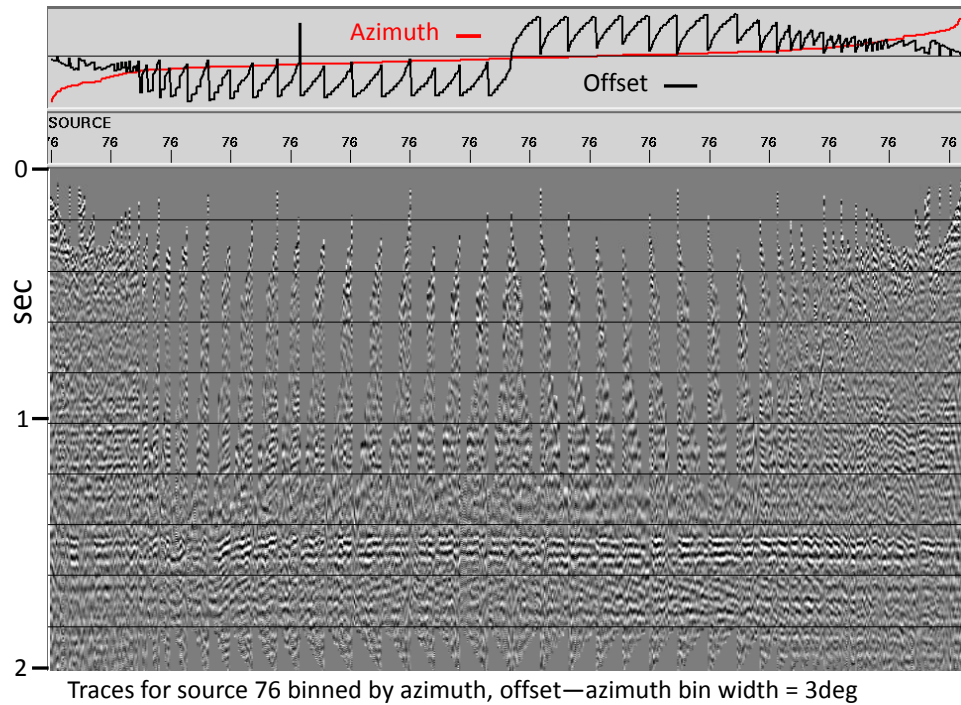


FIG. 11. Azimuthal binning scheme in Figure 10 used to bin NMO-corrected traces in source gather 76, with a bin segment width of 3deg. Azimuth bin number and offset distribution plotted above. Note that ~20% of all azimuth bins contain too few traces to transform.

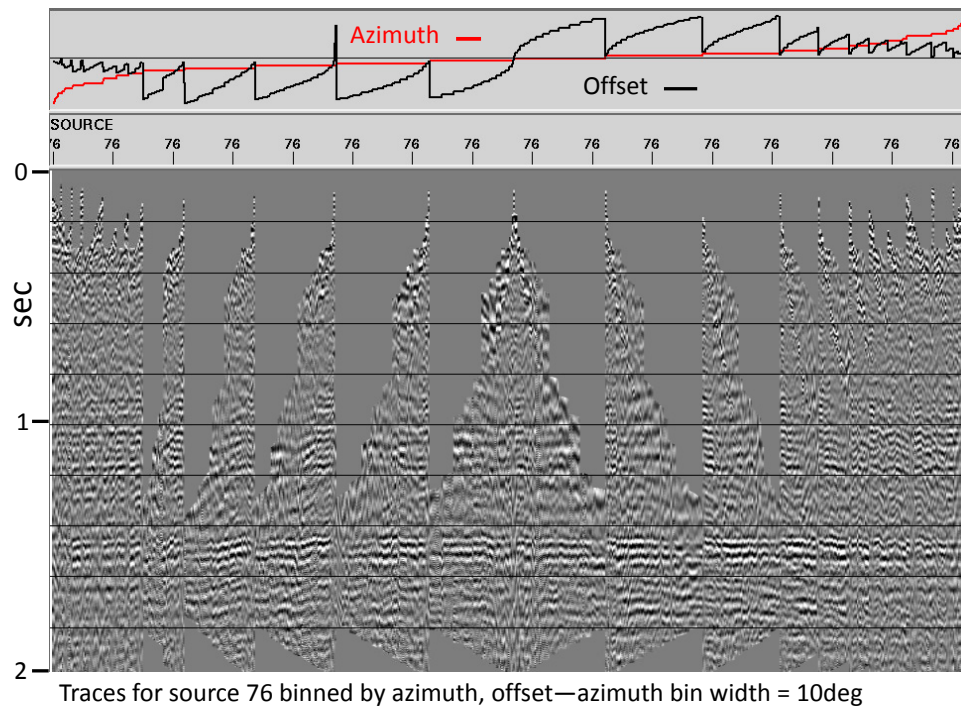


FIG. 12. Azimuthal binning scheme in Figure 10 used to bin NMO-corrected traces in source gather 76, with a bin segment width of 10deg. Azimuth bin number and offset distribution plotted above. Note that ~20% of all azimuth bins still contain too few traces.

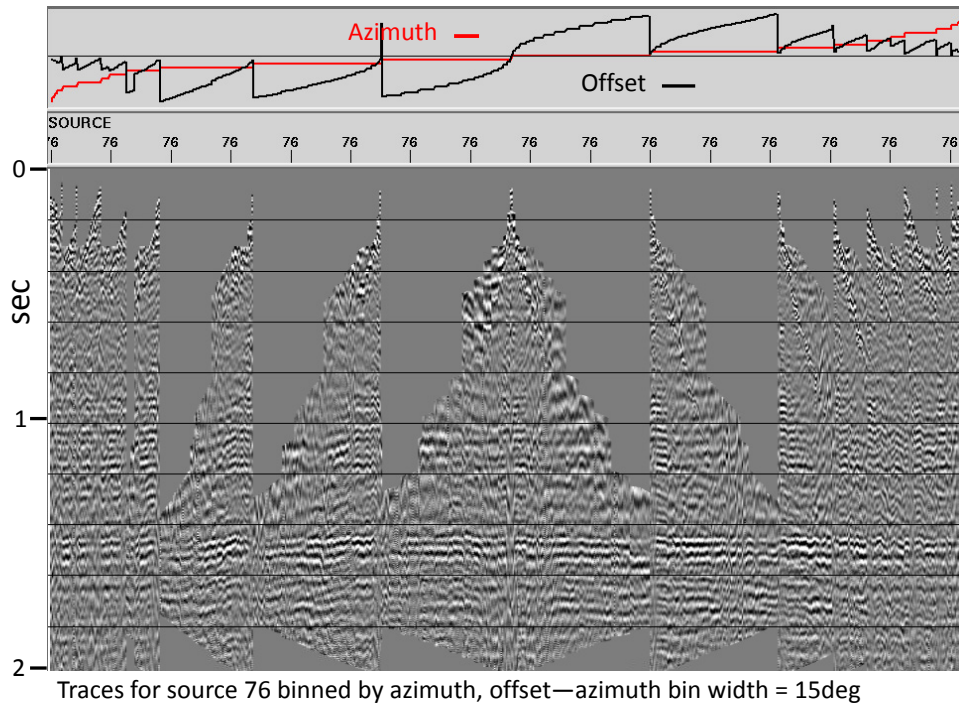


FIG. 13. Azimuthal binning scheme in Figure 10 used to bin NMO-corrected traces in source gather 76, with a bin segment width of 15deg. Azimuth bin number and offset distribution plotted above. Note that ~15% of all azimuth bins still contain too few traces.

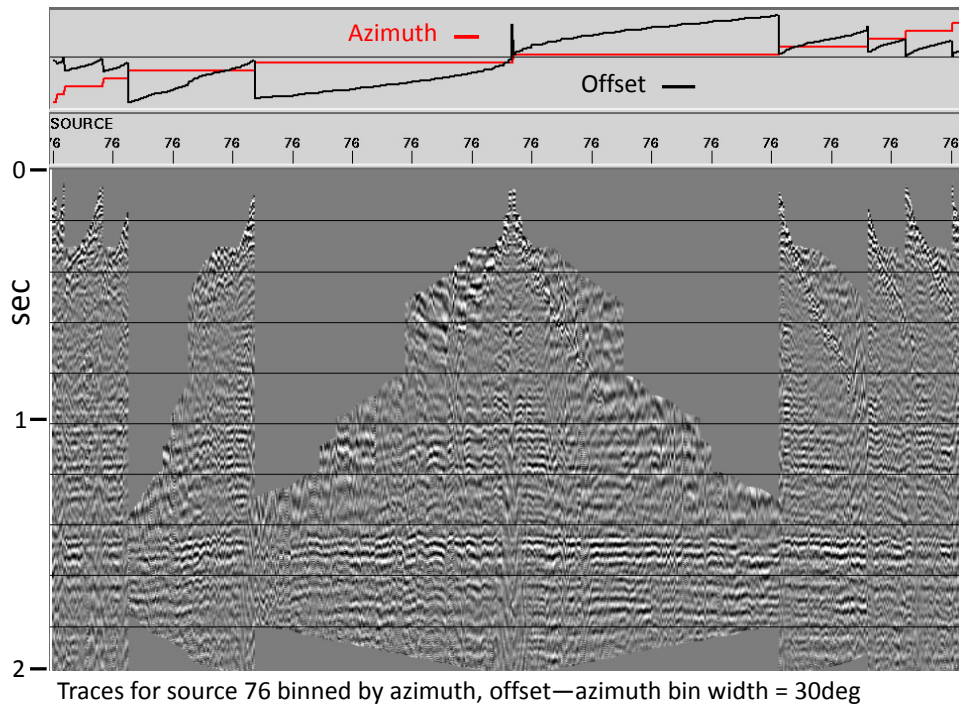


FIG. 14. Azimuthal binning scheme in Figure 10 used to bin NMO-corrected traces in source gather 76, with a bin segment width of 30deg. Azimuth bin number and offset distribution plotted above. Note that only about ~5% of all azimuth bins now contain too few traces. This segment width should be acceptable.

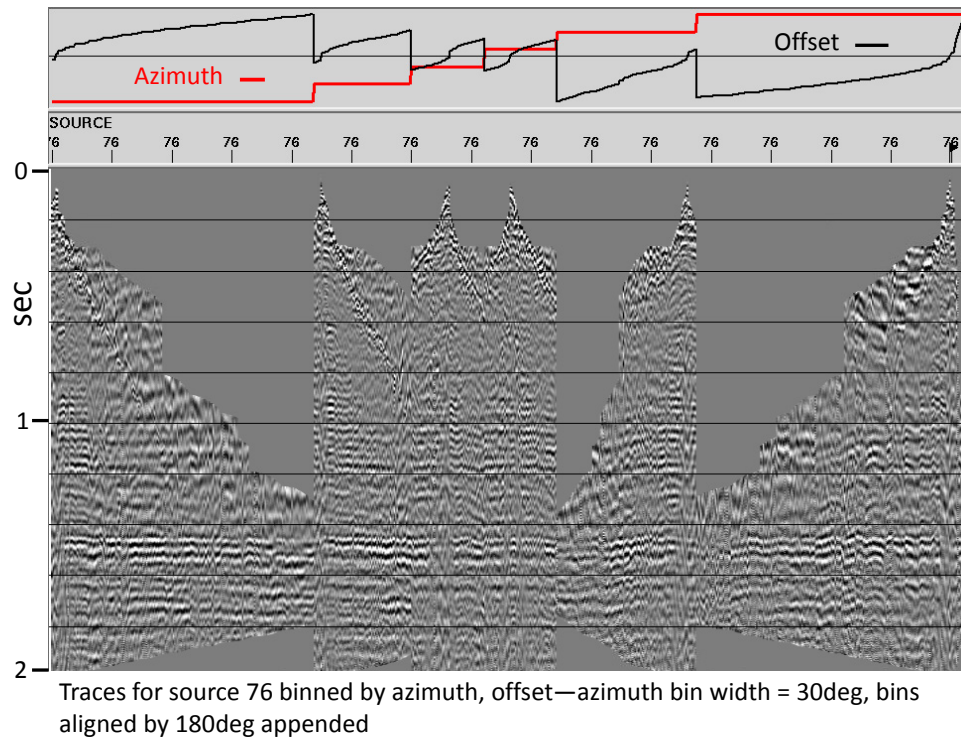


FIG. 15. Azimuthal binning scheme in Figure 10 used to bin NMO-corrected traces in source gather 76, with a bin segment width of 30deg. Bins aligned 180deg apart were then appended, resulting in 6 well-populated ‘super-bins’ with relatively linear offset distributions.

An important aspect of creating ensembles for transform to the RT domain is the fact that using the azimuth bin as a selection parameter removes the large gap in ‘signed offset’ displayed by the receiver line gathers. The signed offset gap disappears because the traces in the receiver line gather on either side of the ‘gap’ are placed in different ensembles due to their differing azimuths. The signed offset is shown as a header plot in Figures 8 and 9. The large gaps can be seen as the large ‘jumps’ between negative and positive offsets on either side of the projected source position, rendering the entire offset distribution for each of these receiver line gathers very non-linear. For the purposes of surface wave filtering, this doesn’t matter, since the noise is estimated in the RT domain, then subtracted from the undisturbed data in the original X-T domain. The linearity of the signed offset header distribution is important for the RT transform itself, however, since offset linearity is assumed for the inverse transform, in the existing algorithm.

The signed offset header appears in a trace header plot in Figures 14 and 15. Note that the offset distributions, while not linear, approach linearity much more closely than those in Figures 8 and 9. This means that radial trace transforms performed on these azimuth-offset gathers will be more nearly invertible. Our existing RT transform is based on the 2D assumption of near-linear offset distributions, and does not retain sufficient trace header information to restore exact offsets (or any other X-T trace headers) to the output of the inverse transform. Hence, a major rewrite of this algorithm will be required if 3D raypath interferometry is to be pursued seriously in the future. For the present study, however, we strive to utilize trace ensembles whose initial offset distribution is as nearly

linear as possible, so that the forced offset linearity of the inverse transform is not too large an error.

Into the raypath-parameter domain

Treating the traces within each azimuth bin, sorted by source-receiver offset, as an ensemble, we apply the RT fan transform to the traces in each bin. For shot number 76, the transforms are shown in Figure 16. Note that the statics are still visible in this domain. In order to impose the common-raypath constraint for raypath interferometry, we next sort the data set by raypath-parameter, azimuth, and source number. Figure 17 shows the common-raypath-parameter ensemble for the raypath-parameter of -997.66. Note that the trace population varies somewhat from azimuth bin to azimuth bin, as a function of source number. This is a consequence of the fact that for each azimuth bin, certain shots or ranges of shots are under-represented at those azimuths due to their location relative to their respective receiver lines. In Figure 17 we also see reflections at all levels, as well as the statics that affect them.

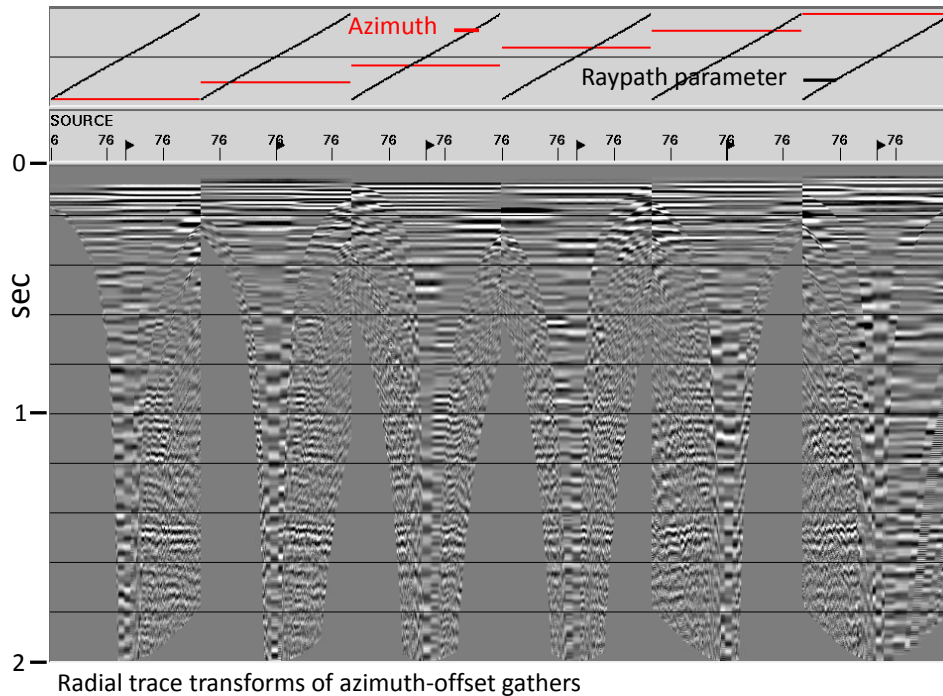


FIG. 16. Radial trace (RT) transforms of the azimuth/offset gathers in Figure 15. Azimuth bin and raypath parameter are plotted above the RT gathers.

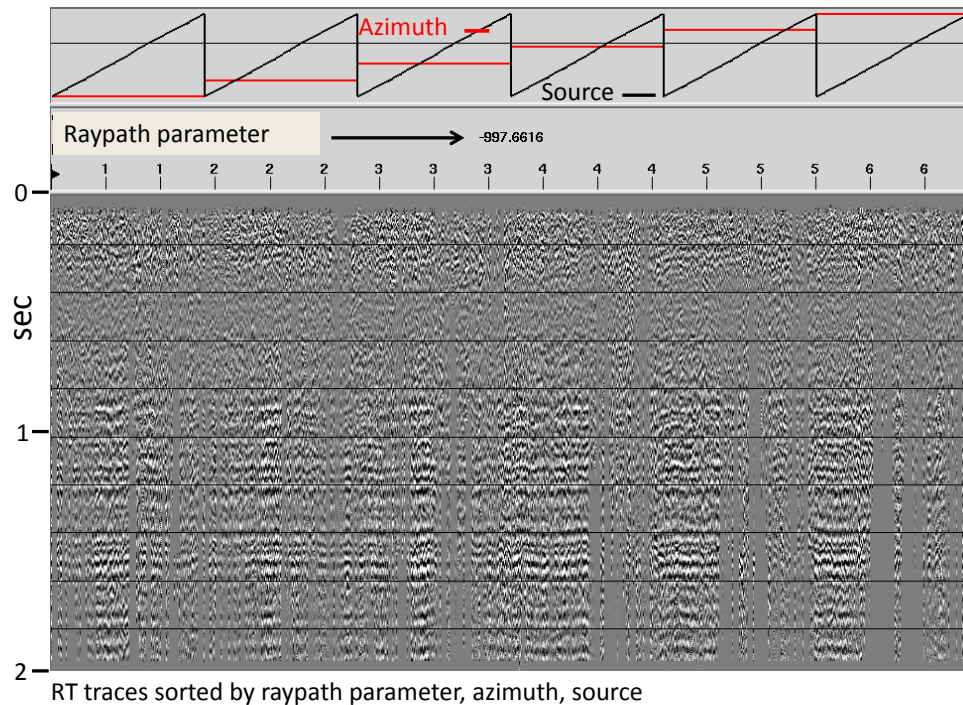


FIG. 17. Raypath-domain traces created by RT transforms of entire Blackfoot data set, sorted by raypath parameter, azimuth, and source location. Only traces for raypath parameter = -987.66 displayed. Azimuth bin and source location number plotted above the RT gathers. Note prominent reflections, which display obvious statics in this domain.

Choice of source as coordinate

While receivers are organized along receiver lines in a mostly orderly progression, source location numbers are sometimes less closely related to actual physical location on the surface of a 3D survey. Since we anticipate smoothing over one or more coordinates of the raypath-parameter ensembles that we create, it seems reasonable that the coordinates we use should have successive surface locations in relatively close proximity. We experimented with sorting 3D ensembles using several source-related trace headers, in order to see which provided the most coherent-looking ensembles. Whether we used coordinates of the source or simply the source location number itself, we could see no particular difference on this data set. Therefore, we chose for this work to simply use the source location number, remembering that for a typical numbering system, the sources will be organized somewhat irregularly along source lines, with physical gaps between the end of one source line and the beginning of another. The physical proximity of traces to their neighbors in a 3D ensemble mainly matters in the reference wavefield estimation step, since that's where the lateral smoothing happens. For a data set like Blackfoot, where the reflections are flat and relatively slowly varying laterally, trace proximity apparently doesn't matter greatly.

We remember that the 3D raypath-parameter ensembles that we created can also be sorted by raypath-parameter, source, and azimuth; in which case, we get a display like that in Figure 18 for the raypath parameter -997.66. We note that in this domain, the trace population is visibly more uniform.

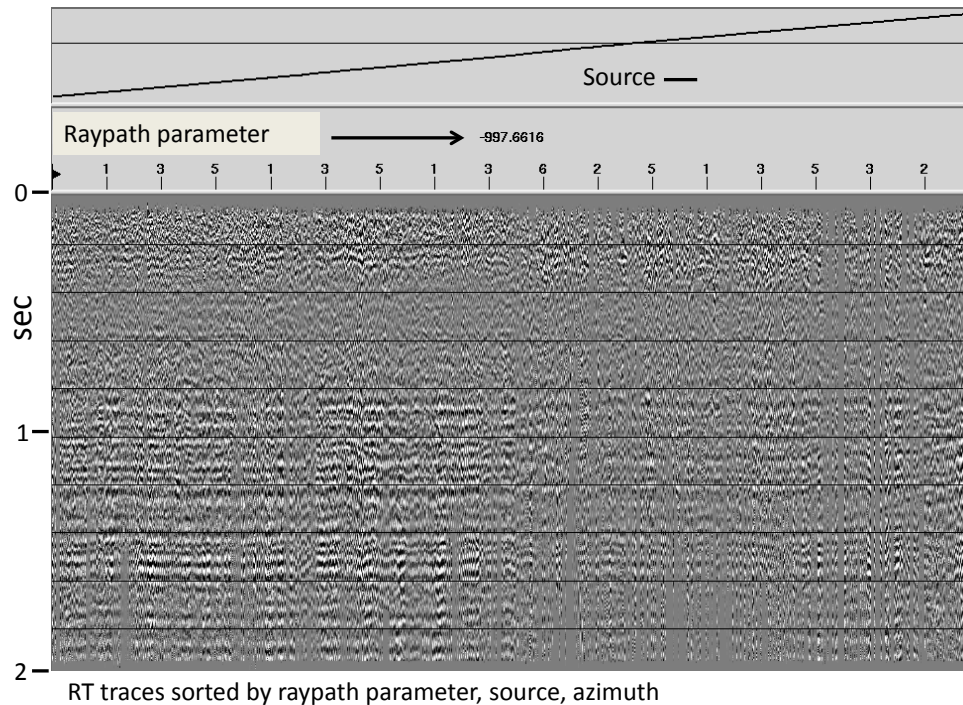


FIG. 18. Raypath-domain traces from the Blackfoot survey sorted by raypath parameter, source location, and azimuth. Only traces for raypath parameter = -987.66 displayed. Source location plotted above the gathers. In this domain, trace distributions are more uniform than in Figure 17. Prominent reflections displaying obvious statics are readily visible.

Reference wavefield estimate

2D domain

The creation of the reference wavefield is one of the key steps in the raypath interferometry technique for estimating and removing near-surface effects from seismic reflection data (Henley, 2012a, 2012b, 2014). As implemented for 2D data processing, the reference wavefield estimation process involves smoothing ensembles of seismic traces along one or more discrete horizons, where these horizons have been selected to coincide with prominent reflections on a preliminary image of the reflection data (Henley, 2012a). Typically, a ‘brute’ CMP stack is created from the raw traces of a 2D seismic survey with no static corrections applied. In this case we assume that the unresolved statics within a CMP trace gather will approximately sum to zero and mainly contribute to broadening the event wavelet representing a reflection. Various reflections visible on the CMP stack image can be ‘picked’ and stored as ‘horizons’. To create a reference wavefield for an ensemble of raw traces, the traces of the ensemble are shifted to flatten the target reflection along its picked horizon, and the traces averaged laterally using a moving average technique called ‘trace mixing’. After smoothing, the horizon shifts are removed, leaving a ‘wavefield estimate’, or ‘pilot trace’ ensemble in which the event waveforms are only slowly varying laterally and are a bandlimited estimate of the reference wavefield that would be measured in the absence of near-surface variations. As shown by Henley (2014), arithmetic averaging can be replaced by other techniques like Singular Value Decomposition and filtering. The main goal is to obtain a trace ensemble with uniform wavelet shape and no short-wavelength timing variations against which to

compare the raw ensemble. Cross-correlations of corresponding traces between a ‘pilot trace ensemble’ and its corresponding raw ensemble, after a ‘conditioning’ step, yield the ‘surface functions’ for each raw trace in the ensemble. Inverse filters derived from the surface functions are subsequently convolved with the raw traces, hence applying the surface corrections. As shown by Henley(2012a), two or more horizon-smoothed pilot trace ensembles can be combined, where structural differences exist between horizons.

3D domain

The reference wavefield estimated in the 2D version of raypath interferometry can be considered to be a projection into the plane of the CMP image of a 3D reference wavefield, which should be a surface varying smoothly in both lateral directions for any continuous reflection interface. This leads naturally to the concept of creating a 3D reference wavefield by smoothing a 3D ensemble in two dimensions. What isn’t quite so clear, however, is how to choose the dimensions over which to smooth the ensembles. In 2D, the choice is relatively obvious, since the RT transform and subsequent trace sorting creates ensembles of constant raypath parameter, with collinear source (or receiver) location as the obvious spatial smoothing dimension. In 3D, however, source (and receiver) location are distributed spatially in linear segments (source lines and receiver lines), and we have added the new dimension of azimuth to the data volume, as well.

One way in which to choose appropriate smoothing dimensions is to examine the visible static jitter between adjacent traces in ensembles selected according to the prospective dimensions. As we indicated in a previous section, transformation to a raypath-parameter domain can be accomplished using the Radial Trace transform, which requires a well-populated input ensemble and a near-linear offset distribution for its most effective operation. As indicated earlier, a group of azimuth-offset gathers created for each source in the survey appears to satisfy these requirements best. Thus, our choice of pre-transform binning parameters according to bin population and other considerations determines the directions available for smoothing in pilot trace creation. Since the ‘offset’ dimension is replaced during the RT transform by raypath-parameter (Figure 16), we have three trace header parameters available for sorting RT traces into ensembles, two of which can be used for smoothing directions. Following the development shown for 2D raypath interferometry (Henley, 2012a), we choose raypath parameter as the principal sort key, so that ensembles will be common-raypath-parameter ensembles. Sorting the traces for a single raypath-parameter by azimuth and source results in an ensemble like that in Figure 17, while sorting the same traces by source and azimuth results in Figure 18.

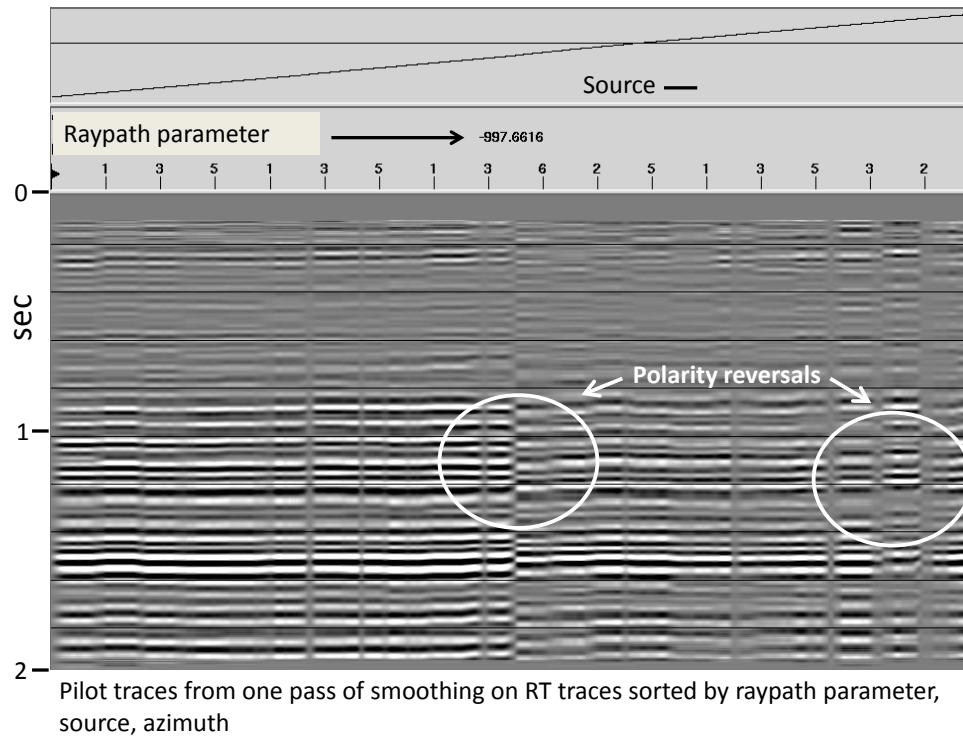


FIG. 19. Wavefield estimate for raypath parameter = -987.66 obtained by lateral smoothing and SVD filtering in the source-location direction on the traces in Figure 18. Obvious polarity reversals and gaps in data are likely due to low trace-fold in input gathers.

Applying lateral smoothing to source-azimuth gathers results in Figure 19, where we can see relatively smooth and continuous reflections with a few obvious breaks and polarity reversals, probably caused by low trace fold in certain portions of the ensemble. Sorting the smoothed results to the azimuth-source domain, we see many more obvious breaks and jitters (Figure 20). Smoothing in the azimuth direction on these ensembles, however, leads to the result shown in Figure 21, where the majority of traces show the same waveform and the pilot traces are missing only in low trace-population zones which are excluded from the smoothing algorithms. Figure 22 shows these results sorted back to source-azimuth. The events are much more continuous and smooth and show none of the polarity reversals of Figure 19. Clearly, the ensembles portrayed in Figures 21 and 22 seem better than those in Figures 19 and 20 as reference wavefield estimates: 2-dimensional smoothing seems to be the right approach for creating smooth reference wavefield estimates. Note that for the current data set, we have not considered the additional complication of flattening reflections to a horizon, since the reflections in the Blackfoot data are so nearly flat.

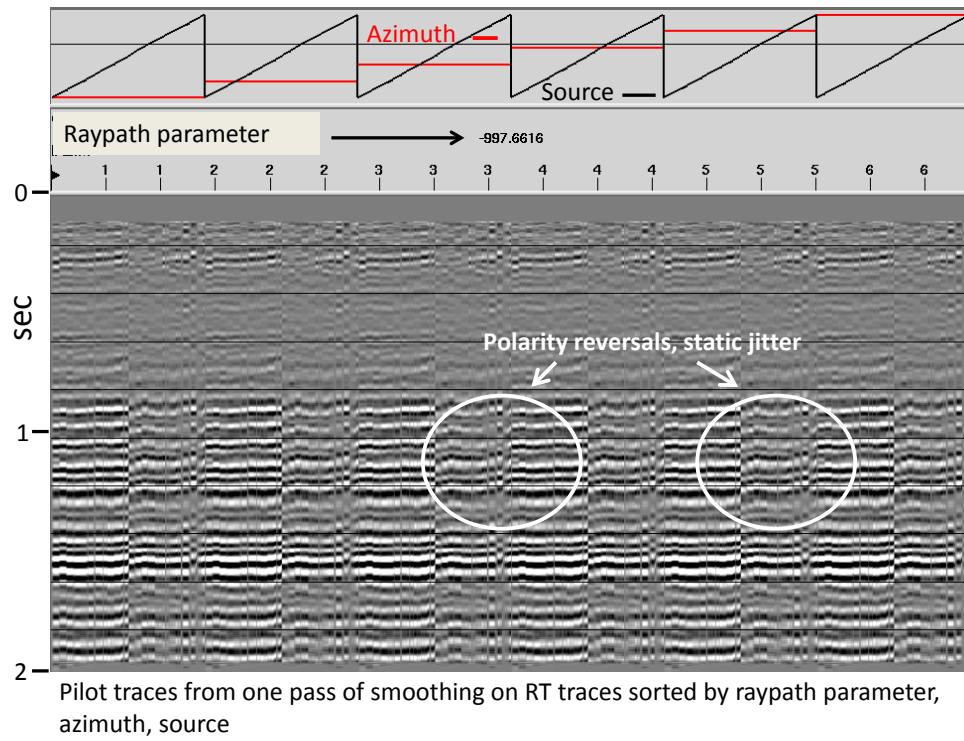


FIG. 20. Traces from wavefield estimate in Figure 19, sorted by azimuth and source location. It is now clear that smoothing only along one dimension (source location) is not adequate for creating a smooth estimated wavefield.

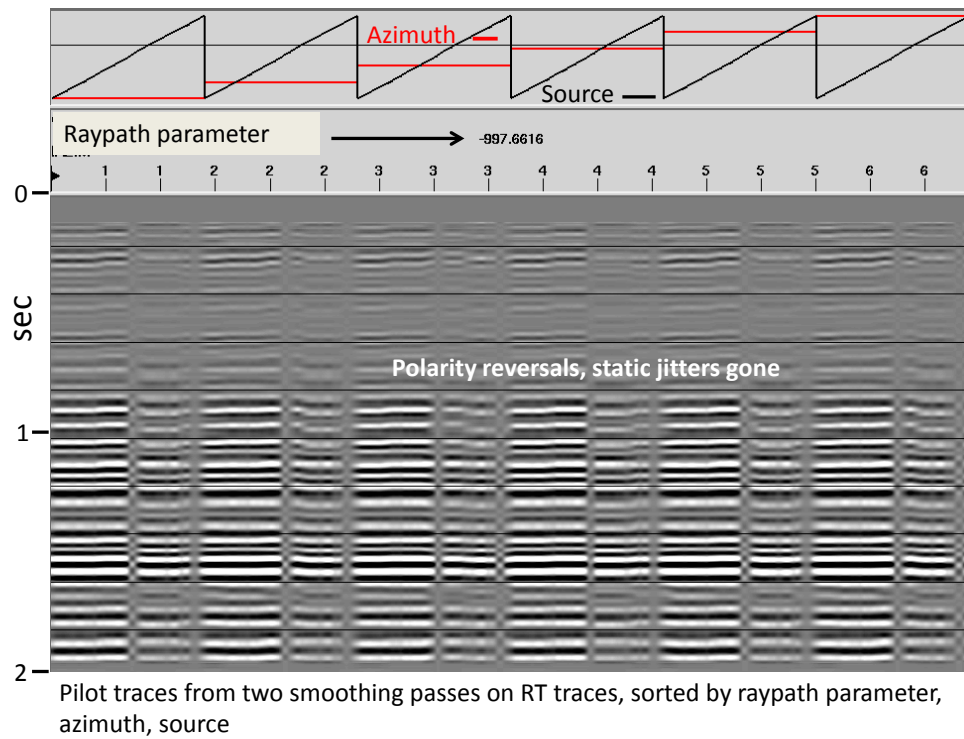


FIG. 21. Wavefield estimate for raypath parameter = -987.66 created by two lateral-smoothing/SVD-filtering passes (along source-location direction, then along azimuth-bin)

direction). Note that while there are more trace gaps in this wavefield estimate, the flatness and smoothness are better than in Figure 20.

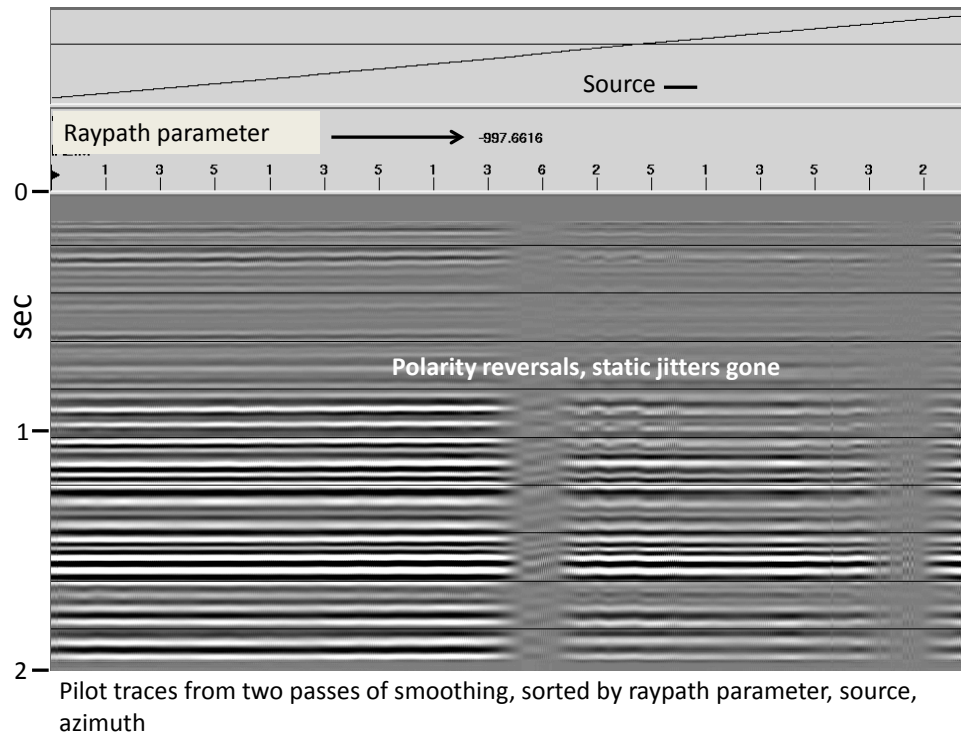


FIG. 22. 2D smoothed wavefield estimate sorted back into source/azimuth-bin order. Note that polarity reversals are gone, and wavefield estimate is much flatter than that in Figure 19.

Applying interferometry

In Figure 23, we show a small sample of pairs of corresponding raw/pilot traces, to show that the pilot traces are both well-aligned and coherent in waveform, and that the shifts and waveform variations in the corresponding raw traces should be easily determined by cross-correlating the trace pairs. Figure 24 shows a small sample of representative ‘surface functions’ (cross-correlations conditioned by raising their amplitudes to an odd power, then weighting with a Hanning Function), and Figure 25 shows the same functions in colour, to better emphasize their amplitudes. From these surface functions, broadband inverse filters are derived, then applied to their corresponding raw RT traces in the source-azimuth gathers to correct the traces for common-raypath surface anomalies.

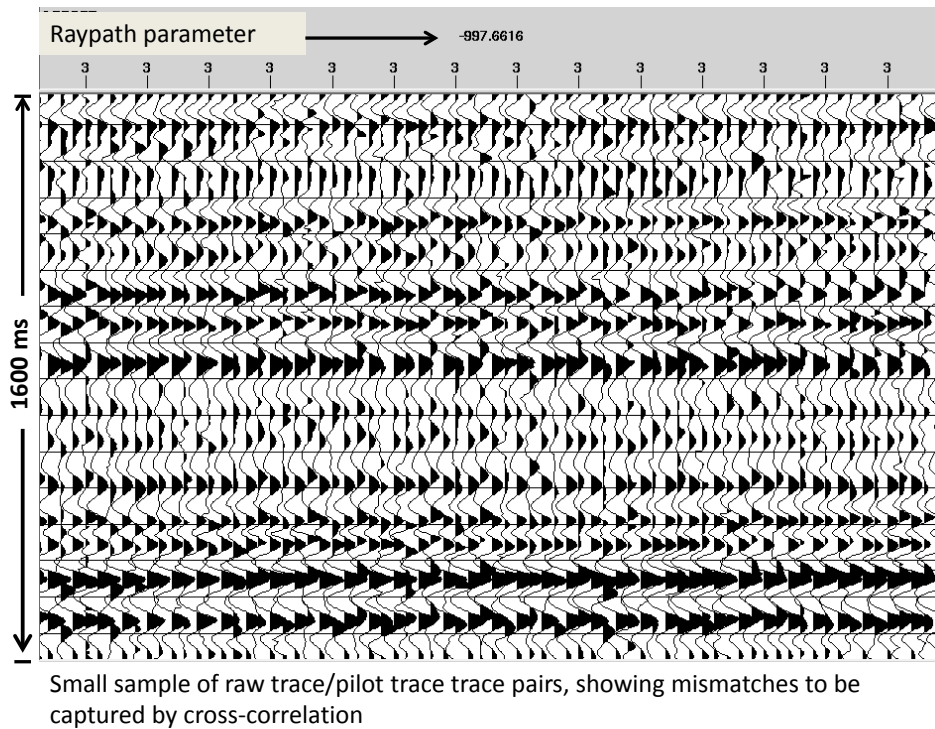


FIG. 23. A small sample of gated raw-trace/pilot-trace pairs. The cross-correlations of pairs like this create all the components of the 3D surface functions (each surface function has coordinates of surface location, raypath parameter, and azimuth bin).

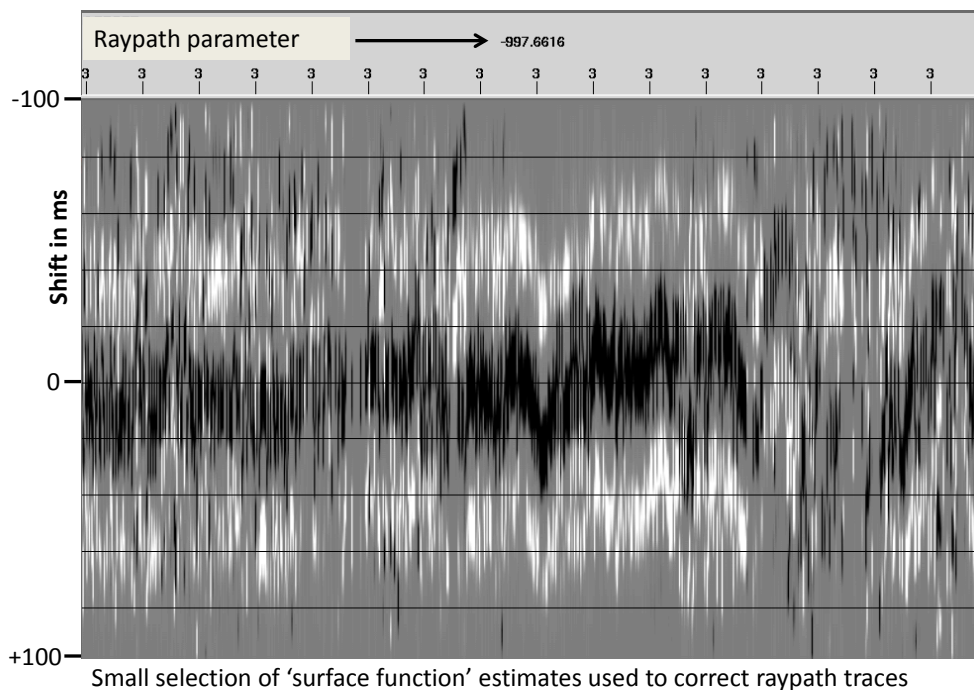


FIG. 24. A small sample of the surface function estimates obtained from cross-correlating raw traces with their corresponding pilot traces, then conditioning the cross-correlations by raising their samples to an odd power and windowing them. Inverse filters are created from these surface functions.

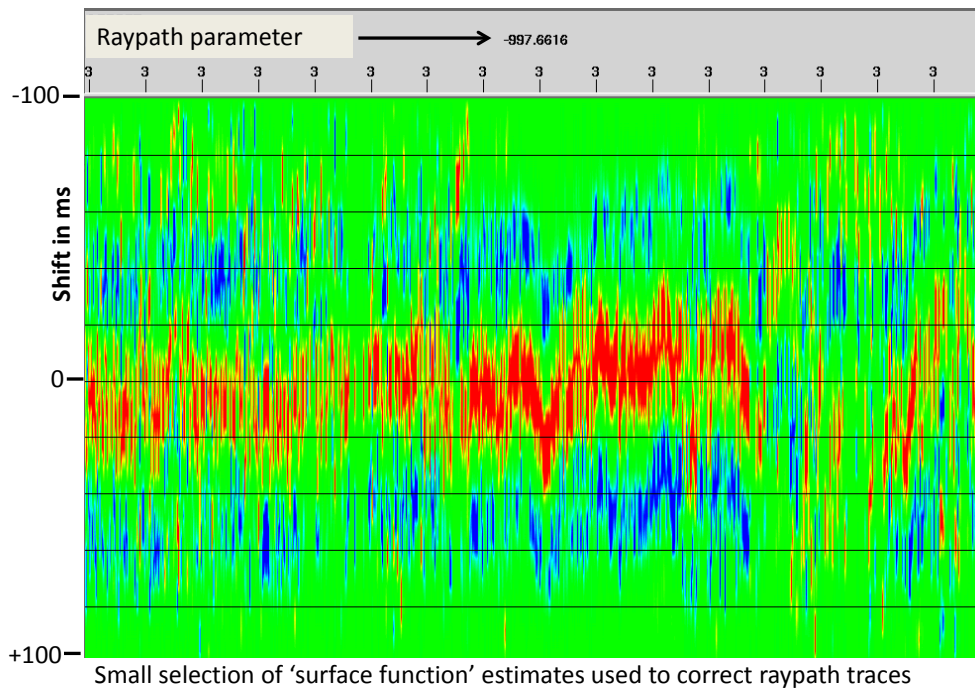


FIG. 25. Colour version of Figure 24. Amplitude dynamic range is more apparent in this display.

Figure 26 shows the common-raypath source-azimuth gather corresponding to Figure 17 after application of raypath interferometry using the reference wavefield estimate smoothed in 2 dimensions, while Figure 27 shows the same gather where the raypath interferometry has used a reference wavefield smoothed in only one dimension. While not dramatically different, the results for 2-dimensional smoothing clearly show flatter reflections at all levels than the raw traces or the results from the 1-D smoothed reference wavefield.

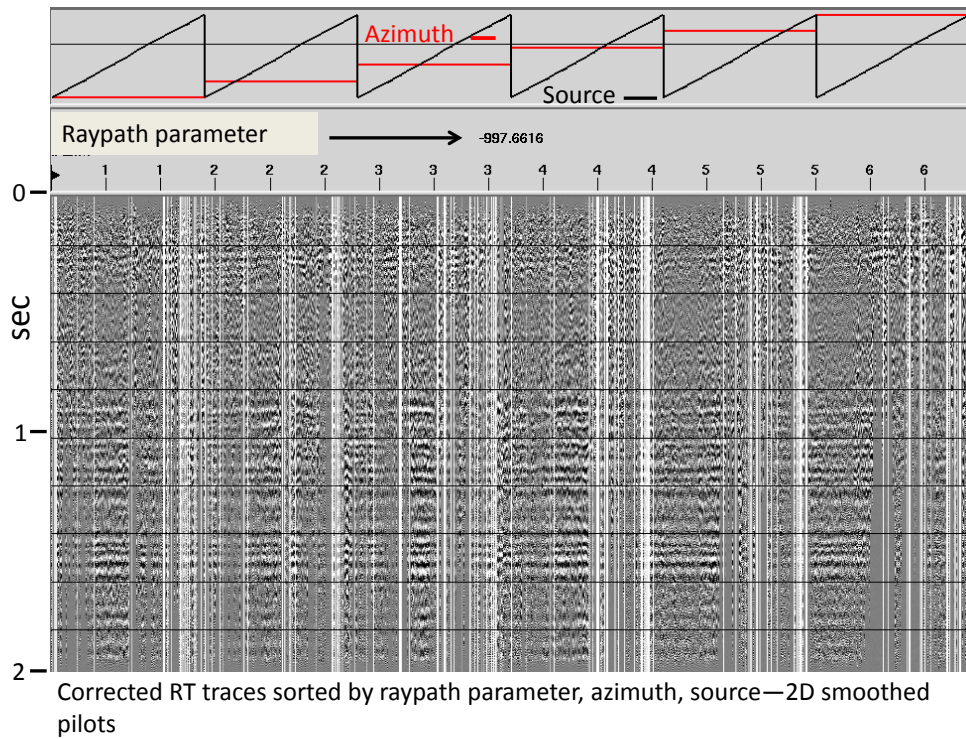


FIG. 26. RT traces from Figure 17 after being corrected by convolution with inverse filters derived from surface functions for the traces. The 2D-smoothed reference wavefield was used for these corrections.

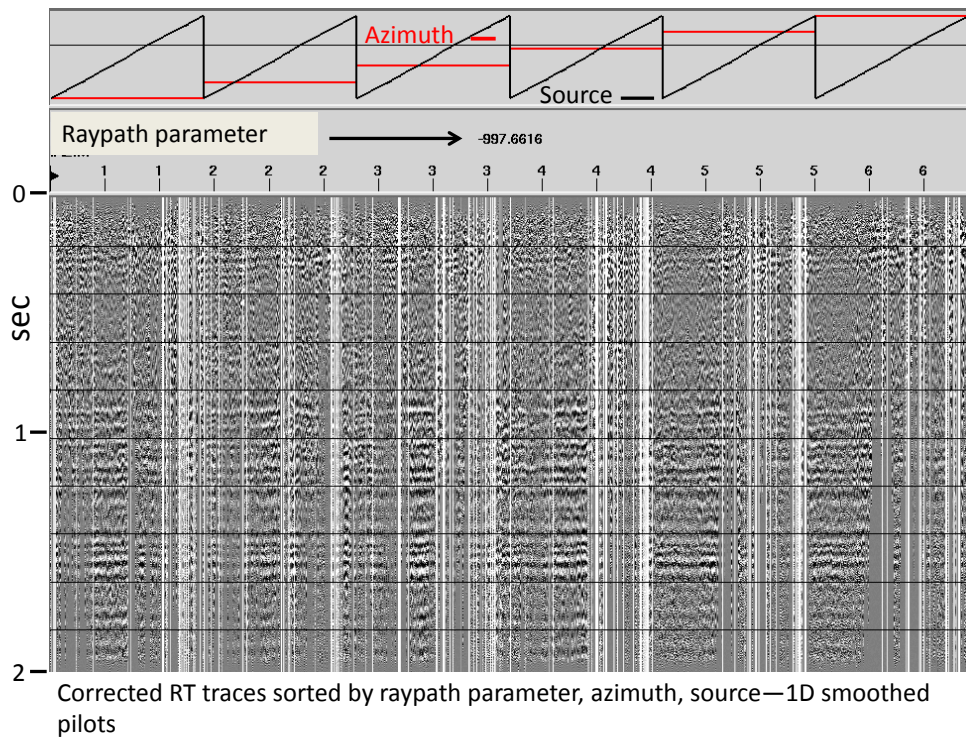


FIG. 27. The RT traces from Figure 17 after being corrected by convolution with inverse filters derived from surface functions estimated using the 1D smoothed reference wavefield. In comparison with Figure 26, residual statics can still be observed.

Figure 28 shows the corrected traces gathered back into RT ensembles, comparable to Figure 16. While the reflections are not perfectly flat, they are clearly flatter than on the original RT transforms and show less static jitter. Inverting these transforms yields the corrected azimuth-offset gathers in Figure 29, comparable to Figure 15 (reproduced as Figure 30), except that the offset distributions in the output X-T gathers are now linear; so the traces do not quite correspond. Nevertheless, the corrected source gather shows significantly reduced static jitter at all reflection levels. Figure 31 shows the prominent reflection band at about 1400ms on the raw azimuth-offset gathers for shot 76 prior to interferometry, while Figure 32 shows the same gathers after 3D raypath interferometry. The missing traces in the latter are due to raypath-parameter limits in the RT transform, and some effects of the linearized offsets can be seen, as well. Overall, however, the statics evident in Figure 31 have been reduced in Figure 32.

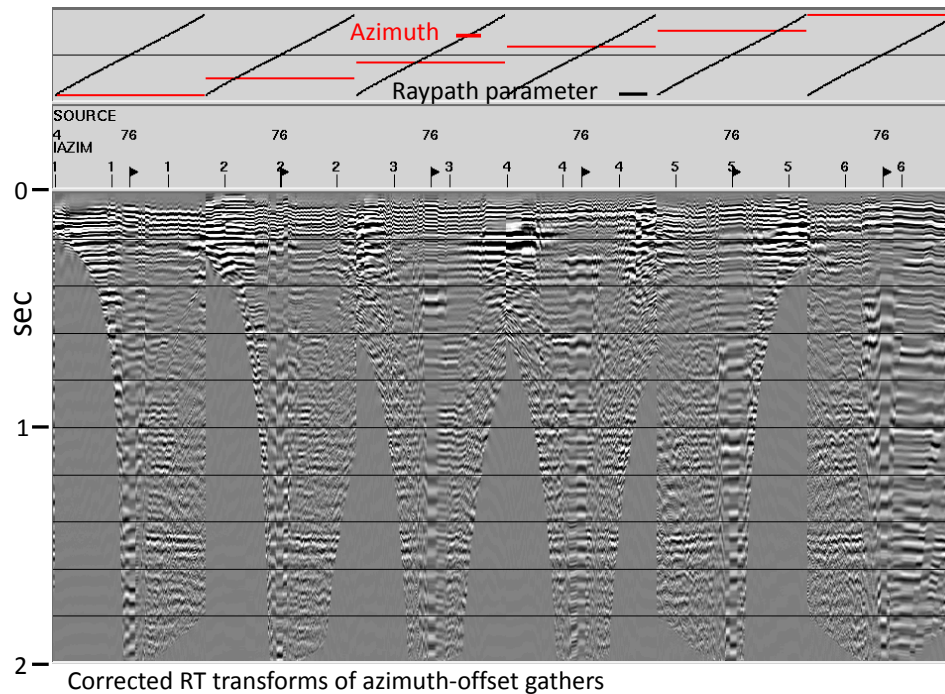


FIG. 28. RT traces, after correction by raypath interferometry with 2D smoothed reference wavefield estimate, sorted back into source-location/azimuth-bin/raypath-parameter and ready to be inverted.

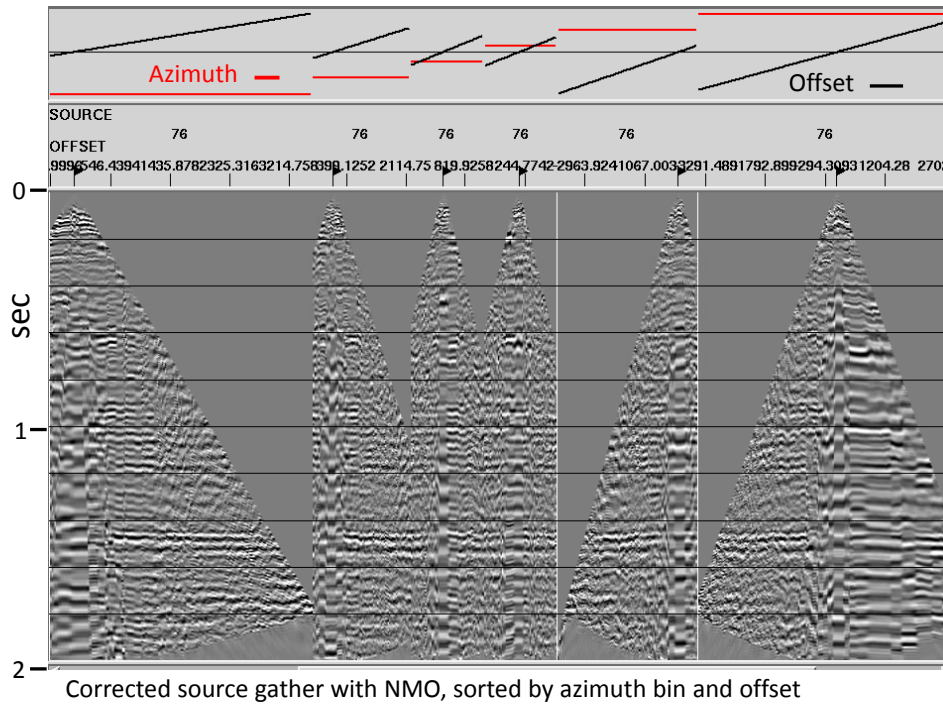


FIG. 29. RT gathers of Figure 28 inverted back to source-location/azimuth/offset gathers. Compare to Figure 30, the uncorrected gathers. The statics are largely corrected, but offset distributions are strictly linear (forced by the inverse RT transform), and trace data are truncated by the raypath-parameter selection criteria of the initial forward RT transform.

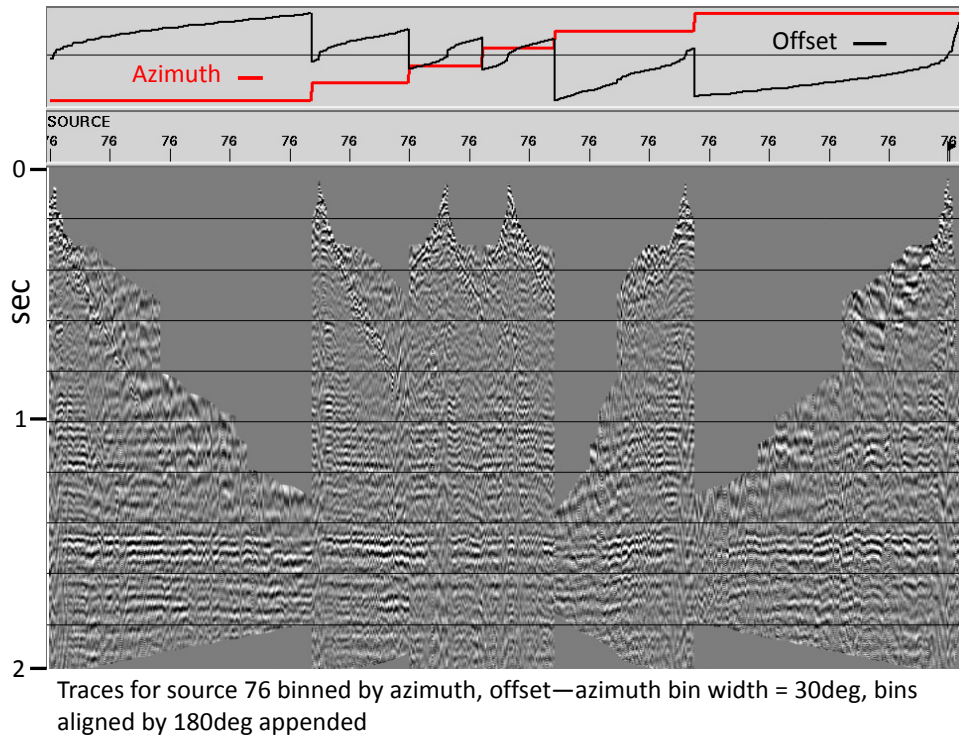


FIG. 30. Same as Figure 15, reproduced here for ease of comparison with Figure 29. Compare offset distributions between Figures 29 and 30, Note that RT transform parameters led to

truncation of early parts of traces (mostly noise and NMO-distorted waveforms). Statics visible in this Figure are mostly gone in Figure 29.

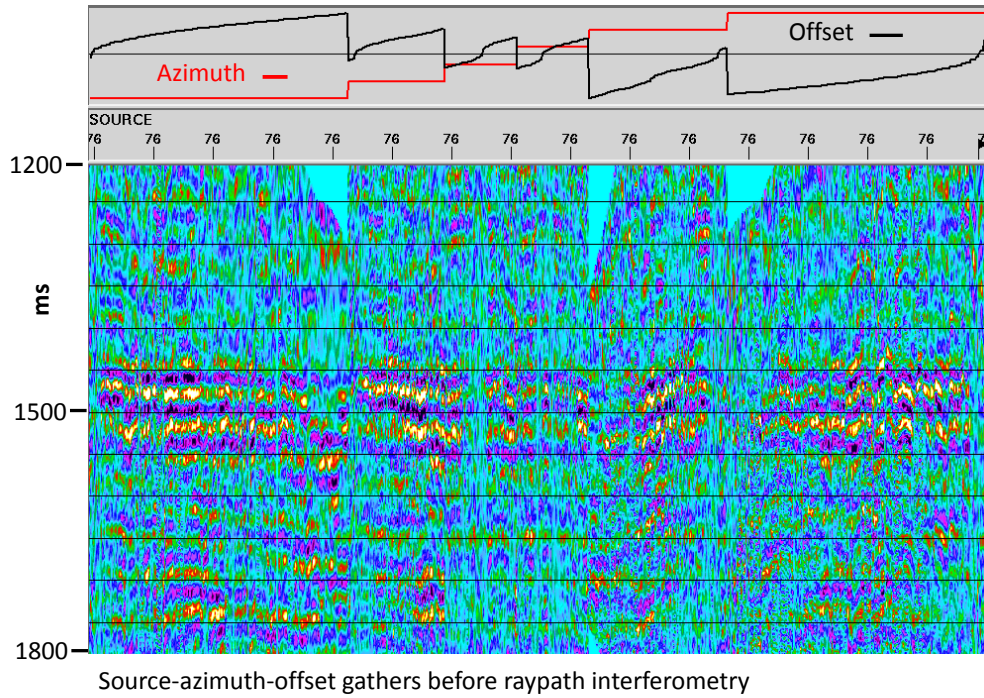


FIG. 31. A zoomed portion of the uncorrected traces in Figure 30.

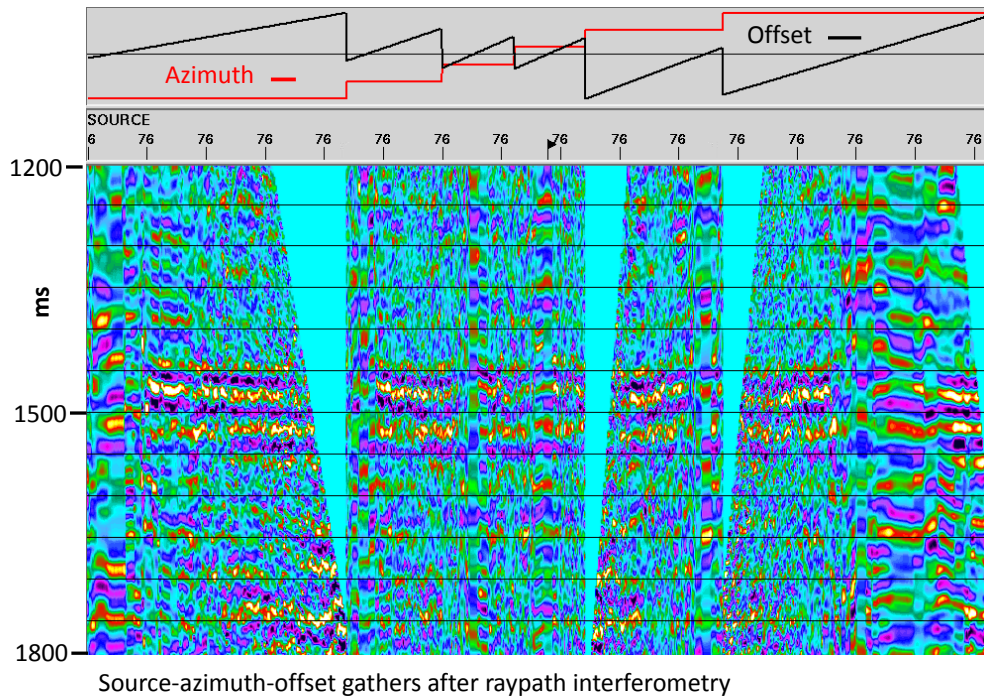


FIG. 32. Zoomed portion of the corrected traces in Figure 29, showing statics largely corrected, in spite of offset distribution distortions that are distorted from the original by the inverse RT transform.

DISCUSSION

Raypath interferometry has been shown to be an effective technique for detecting and removing time and phase anomalies from reflection seismic data due to irregularities in the earth's surface layer. While the effort required for its application may be unjustified for many data sets where the near-surface conditions justify the surface-consistent assumption and hence the application of conventional statics techniques, its use in areas with difficult surface conditions or on data sets with potential for nonstationary corrections (converted wave data, for example) can provide significantly improved results over standard techniques. Since much of the world's land seismic data is now 3D, we have an incentive to extend raypath interferometry to 3D. Whereas determining simple static shifts for 3D seismic traces is a relatively straightforward process, mainly involving 3D binning of traces and using the surface-consistency constraint to guide mathematical computation of statics, 3D interferometry involves other considerations.

One significant consideration is the extension of the 2D surface function, unique to each surface location, introduced for 2D raypath interferometry, to a 3D surface function, also unique to each surface location. While it is conceivable to define such a surface function as a function of rectangular coordinates, it seemed more natural to extend its definition by introducing source-receiver azimuth as a third independent variable. In the new definition, the surface function is a waveform describing the distribution of reflection arrivals for a surface location, where the timing and shape of the function varies with near-surface raypath angle, source-receiver azimuth, and surface location. As with the 2D surface function, which varies only with raypath angle and surface location, the 3D surface function reduces to a single time-shifted spike in the case of single reflection arrivals and surface-consistency.

The introduction of source-receiver azimuth as an independent variable for the surface functions requires introducing the same variable into the data volume in order to allow us to estimate and apply the surface functions. Two further considerations for extending raypath interferometry to 3D are choosing an appropriate transform to a raypath-parameter domain; and choosing a method for estimating the 3D reference wavefield. If we choose to apply the radial trace transform to move the 3D data volume into a raypath-parameter domain, this appears to be fairly straightforward, since the only required parameter is source-receiver offset. However, simply applying the RT transform to receiver line gathers, as is done for radial trace filtering of surface waves, is problematic, since the source-receiver offsets for a general receiver line gather do not share the same azimuth relative to the source, and the resulting offset distribution is highly nonlinear. Fortunately, if we impose the additional geometric parameter of source-receiver azimuth, it is possible to collect ensembles within a particular 3D source gather whose offset distributions are more nearly linear, and whose offset vectors are better aligned. This appears to be an acceptable approximation, at least as shown in this preliminary analysis.

If we were working in rectangular coordinates, the obvious way in which to estimate the reference wavefield, or pilot traces, would be to smooth along picked horizons in two orthogonal directions. However, since we are forced by our choice of raypath-parameter transform and the coordinate system for the 3D surface functions to a radial coordinate system, smoothing is most easily implemented along directions related to those

coordinates. For the flat-lying reflections in our test data set, it appears that smoothing along source location and along azimuth direction can provide a reasonable reference wavefield. If we need to smooth along picked horizons, as in the general case, it is likely that the choice could be more difficult.

We have shown some promising early results for extending raypath interferometry from 2D into 3D, but outstanding questions remain:

- Is there a better raypath-parameter domain?
- Should the data be smoothed in rectangular coordinates before transforming to the raypath-parameter domain?
- Do the apparent improvements seen on azimuth-source gathers lead to better 3D imaging?

ACKNOWLEDGEMENTS

The author thanks CREWES and NSERC for the funding necessary to carry out this work. Conversations with Raul Cova and Kris Innanen are also gratefully acknowledged.

REFERENCES

- Cova, R., Henley, D.C., and Innanen, K.A.H., 2013a, Non-stationary shear wave statics in the radial trace domain, CREWES Research Report, **25**.
- Cova, R., Henley, D.C., and Innanen, K.A.H., 2013b, An interferometric solution for raypath-consistent shear wave statics, CREWES Research Report, **25**.
- Cova, R., Henley, D.C., and Innanen, K.A.H., 2014a, Inverting raypath dependent delay times to compute S-wave velocities in the near surface, CREWES Research Report, **26**.
- Cova, R., Henley, D.C., and Innanen, K.A.H., 2014b, Making shear wave statics actual statics using radial-trace and tau-pi transforms, CREWES Research Report, **26**.
- Cova, R., Wei, X., and Innanen, K.A.H., 2015, Shear wave near-surface corrections in the tau-p domain: a case study, CREWES Research Report, **27**.
- Lawton, D.C., 1996, Design review of Blackfoot 3C-3D seismic survey, CREWES Research Report **8**.
- Henley, D.C., 2007a, Raypath statics revisited: new images, CREWES Research Report **19**.
- Henley, D.C., 2007b, Radial filtering 3D data, CREWES Research Report, **19**.
- Henley, D.C., and Daley, P.F., 2008, Applying interferometry to converted wave statics, CREWES Research Report, **20**.
- Henley, D.C. and Daley, P.F., 2009, Hybrid interferometry: surface corrections for converted waves, CREWES Research Report **21**.
- Henley, D.C., 2012a, Interferometric application of static corrections, *Geophysics*, **77**, No. 1, pp Q1-Q13.
- Henley, D.C., 2012b, Interference and the art of static correction: raypath interferometry at Hussar, CREWES Research Report **24**.
- Simin, V., Harrison, M.P., and Lorentz, G.A., 1996, Processing the Blackfoot 3C-3D seismic survey, CREWES Research Report **8**.